Local orbital frame predictor for LEO drag-free satellites

Acta Astronautica 66 (2010) 446 -- 454

Local orbital frame predictor for LEO drag-free satellite

Enrico Canuto[a], Luca Massotti[b,‡]

[a]*Politecnico di Torino, Dipartimento di Automatica e Informatica, Corso Duca degli Abruzzi 24, 10129 Torino, Italy*

[b]*ESA Earth Observation Programme, Future Missions Division, ESTEC EOP-SF, Noordwijk NL-2200 AG*

Abstract

This paper is concerned with the on-board real-time position and rate prediction of the spacecraft centre-of-mass as input data to local orbital frame (LORF) determination for Low-Earth Orbit drag-free satellites. Study and simulation results are justified by Drag-Free and Attitude Control of the GOCE satellite (Gravity field and steady-state Ocean Circulation Explorer), the LORF being the instantaneous reference for satellite attitude and scientific data. The paper focuses on modeling issues in view of disposing of an accurate orbit dynamics at lower frequencies, which is effective in reducing integration errors because of a narrow-band filter requested by the wide-band measurement errors. A further remedy in this sense is the addition of a second order disturbance dynamics leaving unexplained bounded noise components. Simulated results are presented with reference to the GOCE mission.

Keywords: Local orbital frame, prediction, drag free satellite, GPS.

1 Acronyms

CoM = Centre-of-Mass

GOCE = Gravity field and steady-state Ocean Circulation Explorer

GPS = Global Positioning System

‡ Corresponding author
E-mail addresses: Enrico.Canuto@polito.it (E. Canuto)
Luca.Massotti@esa.int (L. Massotti)

LEO = Low-Earth Orbit

LORF = Local Orbital Reference Frame

LTI = Linear Time Invariant

MBW = Measurement BandWidth

PSD = Power Spectral Density

RMS = Root Mean Square

2 Nomenclature

$\mathbf{a}_d$ = perturbing accelerations

$\mathbf{d}_k$ = unknown disturbance source driven by white noise

$\boldsymbol{e}_0$ = Local Orbit Reference Frame orientation error vector

f = Fourier frequency

$\mathbf{g}$ = local gravity acceleration vector

L = observer gain matrix

$\partial\mathbf{P}$ = error dynamics

$\boldsymbol{r}$ = inertial position of the satellite CoM

S = Power Spectral Density

U = Earth's gravitational potential

$\boldsymbol{v}$ = velocity of the satellite CoM

$\mathbf{v}_r$, $\mathbf{v}_v$ = GPS error vectors

$\mathbf{w}$ = white noise vector

$\mathbf{x}_k$ = discrete-time state vector

$\mathbf{y}$ = vector of sampled measurements from GPS

$\mathbf{z}_k$ = disturbance state vector

α_{ki} = orbit angular increment

λ_h = closed-loop eigenvalues

μ = Earth gravitational constant

σ_r, σ_v = standard deviations of GPS position and velocity errors

$\partial\Omega$ = perturbation term of the orbit rate

$\underline{\omega}_O$ = mean orbital angular rate

3 Introduction

This paper is concerned with the on-board real-time estimation and prediction of the spacecraft centre-of-mass (CoM) position and rate as input data to local orbital frame (LORF) determination for LEO (Low-Earth Orbit) drag-free satellites. Study and simulation results are justified by the Drag-Free and Attitude Control of the GOCE satellite (Gravity field and steady-state Ocean Circulation Explorer), the LORF being the instantaneous reference for satellite attitude and scientific data [3, 4, 5]. The GOCE satellite, launched in March 2009, will fly in a near-circular, sun-synchronous orbit ($96.5\,°$ inclination) at a mean geodetic height $h \cong 250$ km, with a mean orbital rate $\underline{\omega}_O \cong 1.17$ mrad/s. The aim is to explore the small-scale spatial components of the Earth gravity field to a resolution of about $\lambda_{\min} \cong 100$ km from the gravity gradient tensor measured by an extremely accurate on-board gravity gradiometer. The gradiometer consists of three orthogonal pairs of 3D ultra-fine accelerometers, each pair being located at the extreme of a stable 1 m arm centered on the spacecraft CoM. The range of the spatial wavelengths λ corresponding to the highest gradiometer sensitivity determines the mission Measurement Bandwidth (MBW) $0.005 \le f \le 0.1$ Hz through

$$\lambda f \cong \underline{\omega}_O (R + h) \cong 7760 \text{ m/s}, \tag{1}$$

where f denotes Fourier frequency and R the Earth equatorial radius. Combination of the gradiometer differential accelerations might in principle recover the Earth gravity gradient by eliminating, as a common term, the drag acceleration affecting spacecrafts like GOCE , orbiting at a low Earth altitude. Actually, uncertainties in the gradiometer scale factors and cross-coupling among different axes impose the satellite to be drag-free and to be accurately aligned to the orbital frame, especially within the MBW.

The drag-free control is in charge of keeping the spectral density of the residual CoM non-gravitational accelerations as well as of the angular accelerations below $25 \text{ nm/s}^2/\sqrt{\text{Hz}}$ and $25 \text{ nrad/s}^2/\sqrt{\text{Hz}}$, respectively. The control exploits the mean CoM and angular accelerations measured by six accelerometers of the gradiometer. The

angular drag-free control must be completed with the attitude control in charge of keeping the gradiometer aligned to the orbital frame, mainly because of the accelerometer low-frequency drift and bias. The latter would misalign the spacecraft attitude by a few radians in less than 10 minutes. The attitude control employs star tracker measurements. The LORF, being the reference frame to be tracked by the spacecraft body frame, must be estimated in real-time at an accuracy compatible with the attitude. Similar to acceleration, attitude requirements are stringent in the MBW, below $8\ \mu\text{rad}/\sqrt{\text{Hz}}$ in terms of spectral density, but they are rather relaxed in terms of peak attitude, that must remain below 0.4 mrad. The latter peak requirement allows attitude spectral components and LORF errors to significantly increase in the frequency BW below 1 mHz.

The LORF is defined as the orientation of the osculating instantaneous orbit with respect to an inertial frame like the Earth-centered Equatorial frame at some date, or with respect to a mean Earth-fixed circular orbit only determined by the spherical Earth gravity. In the latter case, the Euler angles of the LORF-to-mean-orbit transformation can be shown to be combination of the ratios between CoM position and rate perturbations with respect to the mean orbit radius and the absolute orbital speed. Direct LORF determination in the order of microradian would imply CoM position and rate measurement errors below 1 m and 1 cm/s, respectively, at a sampling rate greater than 0.1 Hz. Although space-borne GPS receivers approach this limits at a sampling rate of 1 Hz, position and rate measurements need be filtered to cope with non-stationary GPS errors and to extrapolate the measurements during sampling time as requested by control rates above 1 Hz. The objective is to dispose of a robust algorithm, free of measurement statistics, and tuned to quite conservative GPS errors as shown in Table 1.

Table 1

GPS timing and errors

Parameter	Unit	Value
Sampling time	s	1
Position error	m	<30 (1σ)
Rate error	m/s	0.03 (1σ)
Bias		negligible
Delay		negligible

On-board GPS data have been extensively used for several purposes: among them, real-time and a-posteriori orbit determination [7], attitude determination, relative positioning and time synchronization. A survey can be found in [2].

LORF estimation and prediction may be approached through Kalman filtering techniques, which require knowledge of noise statistics and accurate models of orbit dynamics and perturbations. The approach adopted here follows the Embedded Model technique [4]: it starts from an accurate model of the orbit (or controllable) dynamics including eccentricity and J_2 gravity term, which is completed by a disturbance dynamics in charge of estimating model uncertainties and simplifications, neglected gravity anomalies and drag-free control residuals. Key steps are the selection of the disturbance dynamic order, of the size and location of the driving noise. The latter acts as the feedback channel where to update and stabilize the model state variables. The order is designed to match the spectral density of the higher-order gravity anomalies, in agreement with the Kaula's rule [1]. The resulting discrete-time state equations, the Embedded Model, is then completed with the uncertain error dynamics, not be included in the algorithms, but to a-priori guarantee error stability in the tuning of feedback gains. Figure 1 shows the main components to be detailed in the paper. The Embedded Model and the error dynamics are treated in Section 5. When, at the current time, the disturbance driving noise is estimated (not predicted) by the plant measurements through the model error, i.e. the difference between measures and model output, the Embedded Model becomes a state observer. In other terms, state variables are improved (estimation) and predicted. Unknown discrepancies between estimated and 'actual' disturbance collect under 'residuals'.

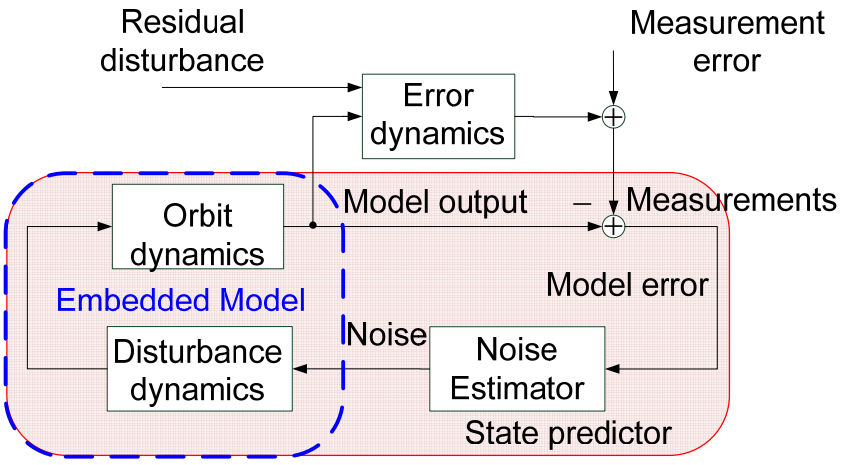

Fig. 1. Block-diagram of the Embedded Model and errors in the form of a state observer.

4 Reference frames and Requirements

The inertial frame $\mathcal{R}_J = \{O, \mathbf{i}_J, \mathbf{j}_J, \mathbf{k}_J\}$ centered in the Earth CoM O, is the equatorial frame at the date J2000. The LORF $\mathcal{R}_O = \{C, \mathbf{i}_O, \mathbf{j}_O, \mathbf{k}_O\}$, centered in the spacecraft CoM C, is defined by the instantaneous orbit orientation, and specifically by the motion direction $\mathbf{v}/|\mathbf{v}|$ of the CoM, $\mathbf{v}$ being the inertial velocity, and by the orbital angular momentum $\mathbf{h} = m_s \mathbf{r} \times \mathbf{v}$, m_s denoting the spacecraft mass and $\mathbf{r}$ the CoM position (Fig 2). The LORF is the reference frame for science measurements and attitude control. The LORF axes are defined by

$$\mathbf{i}_O = \mathbf{v}/|\mathbf{v}|, \mathbf{j}_O = \mathbf{r} \times \mathbf{v}/|\mathbf{r} \times \mathbf{v}|, \mathbf{k}_O = \mathbf{i}_O \times \mathbf{j}_O . \tag{2}$$

The axes from $\mathbf{i}_O$ to $\mathbf{k}_O$ are referred to as along-track, out-of-plane and radial, respectively.

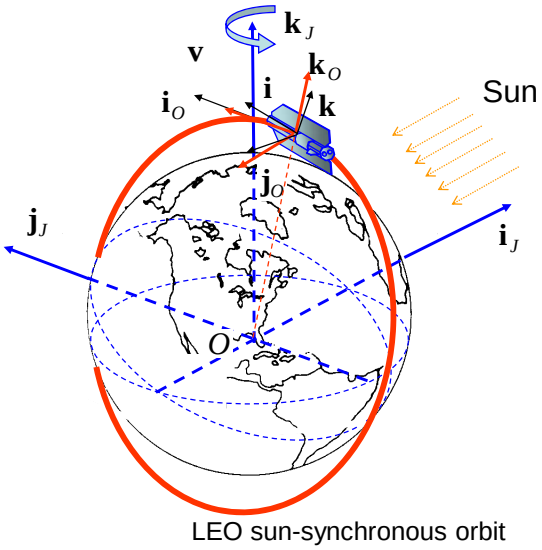

Fig. 2. LEO sun-synchronous orbit and reference frames.

The matrix $\mathbf{R}_O = [\mathbf{i}_O \quad \mathbf{j}_O \quad \mathbf{k}_O]$ accomplishes the LORF-to-inertial coordinate transformation, and defines the reference attitude to be tracked by the spacecraft. The orientation error $\mathbf{e}_O$, caused by the on-line estimate $\hat{\mathbf{R}}_O$, can be defined as

$$\begin{aligned}&\mathbf{R}_O\mathbf{E}_O=\hat{\mathbf{R}}_O,\ \mathbf{E}_O\cong I+\Delta\mathbf{E}_O\\&\Delta\mathbf{E}_O=\begin{bmatrix}0&-e_{Oz}&e_{Oy}\\e_{Oz}&0&-e_{Ox}\\-e_{Oy}&e_{Ox}&0\end{bmatrix},\ \mathbf{e}_O=\begin{bmatrix}e_{Ox}\\e_{Oy}\\e_{Oz}\end{bmatrix}.\end{aligned}\tag{3}$$

Assuming a near-circular circular orbit, $\mathbf{e}_O$ can be shown to be related to inertial position and velocity estimation errors $\Delta\mathbf{r}$ and $\Delta\mathbf{v}$ through

$$\mathbf{e}_O\cong\frac{1}{\underline{r}}\begin{bmatrix}-\Delta\mathbf{r}\cdot\mathbf{j}_O\\\Delta\mathbf{r}\cdot\mathbf{i}_O-\Delta\mathbf{v}\cdot\mathbf{k}_O/\underline{\omega}_O\\\Delta\mathbf{v}\cdot\mathbf{j}_O/\underline{\omega}_O\end{bmatrix},\underline{r}=R+h,\ \underline{v}=\underline{\omega}_O\underline{r},\tag{4}$$

where $\underline{\omega}_O=\sqrt{\mu/\underline{r}^3}\simeq 1.2$ mrad/s is the mean orbital rate, and $\underline{f}_O=(2\pi)^{-1}\underline{\omega}_O\cong 0.19$ mHz the relevant frequency.

Assume now the LORF matrix to be directly measured from GPS measurements

$$\begin{aligned}&\mathbf{y}_r(t_j)=\mathbf{r}(t_j)+\mathbf{v}_r(t_j)\\&\mathbf{y}_v(t_j)=\mathbf{v}(t_j)+\mathbf{v}_v(t_j),\ t_j=jT_g\end{aligned},\tag{5}$$

which are collected from GPS at a uniform sampling rate $f_g=1/T_g=1$ Hz. Properties of GPS errors $\mathbf{v}_r$ and $\mathbf{v}_v$ are not recalled here (see [7]), but they are assumed to be bounded by a discrete-time white and Gaussian noise, and their components to be statistically independent. Assume position and rate errors to be bounded as in Table 2, and denoted their standard deviations with σ_r and σ_v, respectively. Then, replacing position and velocity errors in (4) with the GPS errors in (5), which corresponds to assume the equality

$$\Delta\mathbf{r}(t_j)=\mathbf{v}_r(t_j),\ \Delta\mathbf{v}(t_j)=\mathbf{v}_v(t_j),\tag{6}$$

leads to the following white noise PSD components

$$\begin{aligned}&\begin{vmatrix}S_{Ox}\\S_{Oy}\\S_{Oz}\end{vmatrix}(f)\cong\frac{\sqrt{2T_g}}{\underline{r}}\begin{bmatrix}\sigma_r\\\sqrt{\sigma_r^2+(\sigma_v/\underline{\omega}_O)^2}\\\sigma_v/\underline{\omega}_O\end{bmatrix}\le\begin{bmatrix}6.5\\8.5\\5.5\end{bmatrix}\frac{\mu\text{rad}}{\sqrt{\text{Hz}}},\\&|f|\le 0.5f_g=0.5\text{Hz}\end{aligned}\tag{7}$$

one for each LORF error component in (3). The acronym PSD means the root of the unilateral power spectral density, throughout.

Requirements to LORF estimation errors derive from the spacecraft attitude as the latter is defined by the body-to-LORF transformation. LORF errors should be a fraction of the residual attitude as shown in Table 2, derived from the GOCE requirements.

Table 2

Bounds to LORF errors and attitude

Variable	Overall RMS [μrad]	MBW PSD $\left[\mu\text{rad}/\sqrt{\text{Hz}}\right]$
LORF error	200	4.3
Attitude	370	7.9

The most stringent requirements in Table 2 occur in the MBW. The direct LORF measurement, being not compliant according to (7), justifies a real-time filter for recovering requirements with some margin. The filter will be designed in the form of a state observer around a stylized discrete-time dynamics called Embedded Model, as suggested in [4].

5 The Embedded Model

First, orbit dynamics is derived in continuous-time. An alternative is to use local coordinates with respect to a circular orbit, which provides a version of Hill's equation; this way is not pursued here. The discrete-time model is derived for each inertial coordinate by exploiting their weak interactions due to a near-circular orbit and a near-spherical gravity field.

5.1 Orbit Dynamics

Let us assume the LEO satellite is free-falling, i.e. a drag-free control cancels non-gravitational forces below a certain threshold. Then denote the residual non gravitational CoM acceleration, ideally held to zero, with $\mathbf{a}$. The

inertial position $\mathbf{r}^T = \begin{bmatrix} x & y & z \end{bmatrix}^T$ is related to the Earth-fixed coordinates through longitude λ, latitude θ and radius $r = |\mathbf{r}|$. Denote the Earth's gravitational potential with $U(r,\lambda,\theta)$; the latter is usually expanded into complex spherical harmonics $\bar{Y}_{nm}(\theta,\lambda)$ of degree *n* and order *m*, representing the combination of tesseral and zonal components of the geo-potential model, scaled by the complex spectrum $\bar{K}_{nm}$. By restricting the U expansion to spherical and 2nd order terms, and by confining higher order terms into the anomaly component δU, one obtains

$$U(r,z) = \frac{\mu}{r}\left(1 - \frac{3}{2}J_2\left(\frac{R}{r}\right)^2\left(\left(\frac{z}{r}\right)^2 - \frac{1}{3}\right)\right) + \delta U\,, \tag{8}$$

where $J_2 \simeq 1.08\times10^{-3}$ accounts for the equatorial bulge, R is the equatorial Earth radius, and the explicit terms in (8) are independent of the Earth's rotation.

The gravity acceleration $\mathbf{g} = \nabla U$, derived from (8), is written as follows

$$\mathbf{g} = -\frac{\mu}{r^3}\left(I - \frac{3J_2}{2}\left(\frac{R}{r}\right)^2\left(5\left(\frac{z}{r}\right)^2 I - \Gamma\right)\right)\mathbf{r} + \delta\mathbf{g}\,, \tag{9}$$

where $\Gamma = \mathrm{diag}\{1,1,3\}$, $I = \mathrm{diag}\{1,1,1\}$, and the anomaly $\delta\mathbf{g}(\mathbf{r})$ replaces δU. A further simplification comes by assuming a near-circular orbit as in GOCE. The explicit terms in (9) are expanded around the mean orbit radius $\underline{r} = R + h$ with the care of preserving the perturbing terms of the same order of magnitude as J_2, and of confining residuals into $\delta\mathbf{g}(\mathbf{r})$. That amounts to 1st order expanding the spherical term into

$$-\underline{\omega}_O^2\left(1 + 3\left(1 - \underline{\mathbf{r}}^T\mathbf{r}/\underline{r}^2\right)\right)\mathbf{r} \cong -\underline{\omega}_O^2\left(1 + 3\varepsilon\cos\theta\right)\mathbf{r}\,, \tag{10}$$

where $\varepsilon \le 10^{-3}$ is the orbit eccentricity and θ the orbit anomaly; and to zero-th order expanding the flatness terms scaled by J_2. The final expression becomes

$$\begin{aligned} &\mathbf{g}(\mathbf{r}(t)) = -\underline{\omega}_O^2\left(I + \partial\Omega(\mathbf{r})\right)\mathbf{r}(t) + \delta\mathbf{g}(\mathbf{r}) \\ &\partial\Omega(\mathbf{r}) = 3\left(1 - \underline{\mathbf{r}}^T\mathbf{r}/\underline{r}^2\right)I + \gamma_0\left(z/\underline{r}\right)^2 I - \Gamma_1\,. \\ &\gamma_0 = \frac{15}{2}J_2\left(R/\underline{r}\right)^2,\ \Gamma_1 = \frac{3}{2}J_2\left(R/\underline{r}\right)^2\Gamma \end{aligned} \tag{11}$$

Orbit dynamics can then be written as

$$\begin{bmatrix}\dot{\mathbf{r}}\\ \dot{\mathbf{v}}\end{bmatrix}(t)=\begin{bmatrix}0 & I\\ -\underline{\omega}_O^2\left(I+\partial\Omega(\mathbf{r})\right) & 0\end{bmatrix}\begin{bmatrix}\mathbf{r}\\ \mathbf{v}\end{bmatrix}(t)+\begin{bmatrix}0\\ I\end{bmatrix}\mathbf{a}_d(t),\ \begin{bmatrix}\mathbf{r}\\ \mathbf{v}\end{bmatrix}(0)=\begin{bmatrix}\mathbf{r}_0\\ \mathbf{v}_0\end{bmatrix},\qquad(12)$$
$$\mathbf{a}_d(t)=\mathbf{a}(t)+\delta\mathbf{g}(t)$$

having combined residual non-gravitational accelerations and gravity anomalies into $\mathbf{a}_d$. CoM coordinates in (12) are each other connected through the weak perturbing term $\partial\Omega(\mathbf{r})$.

5.2 Discrete-time Dynamics

The Embedded Model according to [4] is consists of two interconnected parts: the controllable and the disturbance dynamics. Here we prefer avoiding the term 'controllable' and replacing it with 'orbit', since no orbit control is treated. The orbit being drag-free, the input to the controllable part is assumed being close to zero except for the gravity acceleration. The latter is partitioned into a position feedback to be part of the orbit dynamics, and into residual components modelled as an unknown disturbance driven by arbitrary signals, which may modeled as white noise vectors..

Consider a time unit $T=T_g/n_g$, with $n_g\geq 1$, and assume $T<<T_O=2\pi/\underline{\omega}_O$, which implies (12) to be slowly varying during T, and the discrete-time version to become time-varying. The generic discrete time is denoted with $t_i=iT$. Formulation is restricted to a single generic CoM coordinate r_k, $k=1,2,3$, and to its increment v_k [m], which components are collected into the state vector $\mathbf{x}_k^T=\begin{bmatrix}r_k & v_k\end{bmatrix}$. The orbit angular increment of the generic coordinate with $\alpha_{ki}=\omega_{ki}T$, ω_{ki} being the time-varying angular rate, is written from (11) as follows

$$\alpha_{ki}^2=\underline{\omega}_O^2T^2\left(I+\partial\Omega_k\left(\mathbf{r}(t_i)\right)\right),\qquad(13)$$

having denoted the k-th element of the diagonal matrix $\partial\Omega$ in (11) with $\partial\Omega_k$.The resulting discrete-time equation holds

$$\mathbf{x}_k(i+1) = A_k(\mathbf{r}(i))\mathbf{x}_k(i) + \mathbf{d}_k(i),\ \mathbf{x}_k(0) = \mathbf{x}_{k0}$$
$$A_k(\mathbf{r}) = \begin{bmatrix} \cos\alpha_{ki} & \dfrac{\sin\alpha_{ki}}{\alpha_{ki}} \\ -\alpha_{ki}\sin\alpha_{ki} & \cos\alpha_{ki} \end{bmatrix},\ \mathbf{d}_k(i) = \int_{t_i}^{t_{i+1}} \begin{bmatrix} \dfrac{\sin(\omega_{ki}(t_{i+1}-\tau))}{\omega_{ki}} \\ T\cos(\omega_{ki}(t_{i+1}-\tau)) \end{bmatrix} a_{dk}(\tau)\,d\tau, \tag{14}$$

where a_{dk} is a coordinate of $\mathbf{a}_d$ in (12).

By exploiting $T << T_O$, (14) can be further simplified in view of real-time computation by replacing trigonometric functions with polynomial expansions up to 2nd order terms in α_{ki}, which yields

$$\begin{bmatrix} r_k \\ v_k \end{bmatrix}(i+1) = \begin{bmatrix} 1-\alpha_{ki}^2/2 & 1-\alpha_{ki}^2/6 \\ -\alpha_{ki}^2 & 1-\alpha_{ki}^2/2 \end{bmatrix} \begin{bmatrix} r_k \\ v_k \end{bmatrix}(i) + \int_{t_i}^{t_{i+1}} \begin{bmatrix} (t_{i+1}-\tau)I \\ T \end{bmatrix} a_{dk}(\tau)\,d\tau\,. \tag{15}$$

Integration in (15) is solved

(i) by defining a disturbance increment $d_k(i)$, in length units [m], as follows

$$d_k(i) = T\int_{t_i}^{t_{i+1}} a_{dk}(\tau)\,d\tau\,; \tag{16}$$

(ii) by dropping the direct effect of a_{dk} on $v_k(i) = r_k(i+1) - r_k(i)$, as it corresponds to time integration of the unique disturbance source $d_k(i)$.

The result is the discrete-time version of a time-varying oscillator having a very long period with respect to the time unit T, and being subject to an acceleration disturbance

$$\mathbf{x}_k(i+1) = A_{ck}(i)\mathbf{x}_k(i) + B_c d_k(i)$$
$$A_{ck}(i) = \begin{bmatrix} 1-\alpha_{ki}^2/2 & 1-\alpha_{ki}^2/6 \\ -\alpha_{ki}^2 & 1-\alpha_{ki}^2/2 \end{bmatrix},\ B_c = \begin{bmatrix} 0 \\ 1 \end{bmatrix}. \tag{17}$$

The state matrix $A_{ck}(i)$ is slowly time-varying with the orbit angular increment α_{ki}, and has eigenvalues slightly off the unit circle, but they will be stabilized by the state observer. The LORF observer (Section 6) is designed to have constant eigenvalues through time-varying feedback gains.

5.2.1 Disturbance dynamics and noise design

Disturbance dynamics is synthesized starting from the experimental PSD of the CoM disturbances [5, 6].

1) Residual non-gravitational acceleration may be approximated as a wide-band noise within the MBW, and therefore is simply modelled as a white noise w_{0k}. Drifts due to accelerometers are instead included in the gravity anomaly dynamics as follows.
2) Gravity anomalies and modelling errors in the spherical and J_2 terms are modelled from the spectral density of the gravity anomalies reported in Fig. 3.
3) At the end, the total disturbance d_k is decomposed into the sum of a white noise w_{0x}, and of two random drifts $\mathbf{z}_k^T = \begin{bmatrix} z_{1k} & z_{2k} \end{bmatrix}$, driven by a pair of white noises w_{1k} and w_{2k}, which are collected together with w_{0k} into $\mathbf{w}_k$.

The resulting disturbance dynamics of a generic coordinate is

$$\begin{aligned} \mathbf{z}_k(i+1) &= A_d \mathbf{z}_k(i) + G_d \mathbf{w}_k(i) \\ \mathbf{d}_k(i) &= B_c d_k(i) = H_c \mathbf{z}_k(i) + G_c \mathbf{w}_k(i) \end{aligned}, \tag{18}$$

and the relevant matrices hold

$$A_d = \begin{bmatrix} 1 & 1 \\ 0 & 1 \end{bmatrix}, G_d = \begin{bmatrix} 0 & 1 & 0 \\ 0 & 0 & 1 \end{bmatrix}, H_c = \begin{bmatrix} 0 & 0 \\ 1 & 0 \end{bmatrix}, \; G_c = \begin{bmatrix} 0 & 0 & 0 \\ 1 & 0 & 0 \end{bmatrix}. \tag{19}$$

The 2nd order dynamics (18) agrees with the Kaula's rule [1], since the latter approximates the amplitude K_n, $n >> 1$, of the higher-degree spectrum of δU in (8) as

$$K_n \simeq 10^{-5} n^{-2}, \;\; K_n = \sqrt{(2n+1) \sum_{m=-n}^{n} \left| \bar{K}_{nm} \right|^2} \; . \tag{20}$$

Replacing n^{-2} in (20) with the Fourier frequency f [Hz] as follows

$$n^{-2} = \left(\frac{\omega_O}{2\pi f} \right)^2 = \left(\frac{f_O}{f} \right)^2, \tag{21}$$

implies the spectral density of the Earth's gravity accelerations to roll off at -40 dB/decade just after the resonances at the 1st and 3rd orbit harmonics due to the J_2 term, which is confirmed by Fig. 3. Spectral densities were obtained from the simulated time profiles of the gravity acceleration anomalies in J2000 coordinates. Experimental coefficients $\bar{K}_{nm}$ up to degree $n = 36$ and stochastic extrapolation up to 1 Hz were employed to the purpose.

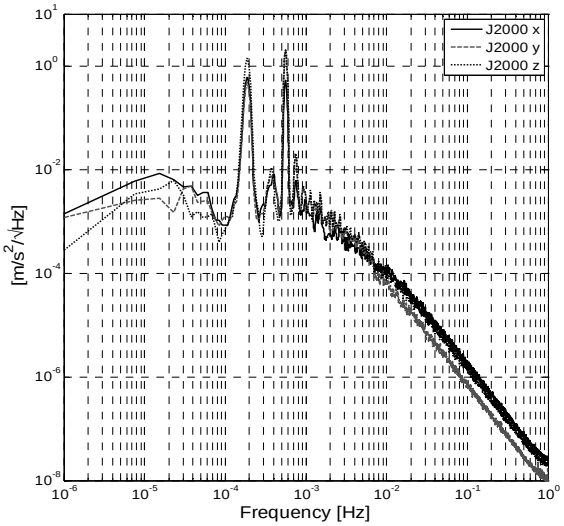

Fig. 3. Simulated PSD of the gravity acceleration anomalies

5.3 Embedded Model and Error Dynamics

The complete model of a single coordinate, obtained by combining (17) and (18), is rewritten by dropping subscript k and adding the subscript m, that stands for model:

$$\begin{aligned}
&\begin{bmatrix}\mathbf{x}_m\\ \mathbf{z}_m\end{bmatrix}(i+1) = F\begin{bmatrix}\mathbf{x}_m\\ \mathbf{z}_m\end{bmatrix}(i) + G\mathbf{w}(i)\\
&\mathbf{y}_m(i) = C\begin{bmatrix}\mathbf{x}_m\\ \mathbf{z}_m\end{bmatrix}(i)\\
&F = \begin{bmatrix}A_c(i) & H_c\\ 0 & A_d\end{bmatrix},\ G = \begin{bmatrix}G_c\\ G_d\end{bmatrix},\ C = \begin{bmatrix}I & 0\end{bmatrix}
\end{aligned} \quad . \tag{22}$$

Note $A_c(i) = A_c\left(\mathbf{r}_m(i)\right)$ depends on the state itself through the perturbing term α_i^2 defined in (13), and the equation size holds

$$\begin{aligned}
&n_y = \dim \mathbf{y}_m = 2,\ n_w = \dim \mathbf{w} = 3\\
&n_c = \dim \mathbf{x} = 2,\ n_d = \dim \mathbf{z} = 2
\end{aligned} \quad . \tag{23}$$

Denote now the vector of the GPS measurements in (5) with $\mathbf{y}(i)$. It is related to the model output $\mathbf{y}_m$ in (22) by the model error $\mathbf{e} = \mathbf{y} - \mathbf{y}_m$, which according to [4] is the composition of the open-loop error dynamics $\partial\mathbf{P}(\mathbf{y}_m,...)$, in fractional form, and of a residual noise $\mathbf{v}$ including GPS measurement errors in (5). The model error relation is written as

$$\mathbf{y}(i) = \mathbf{y}_m(i) + \partial\mathbf{P}(\mathbf{y}_m,...) + \mathbf{v}(i). \tag{24}$$

A state representation of $\partial\mathbf{P}(\cdot)$ can be derived from Eqs. (14), (22) and (24) upon definition of the state and disturbance errors

$$\mathbf{e}_x(i) = \mathbf{x}(i) - \mathbf{x}_m(i),\ \mathbf{e}_d(i) = \mathbf{a}(i) - \mathbf{d}(i). \tag{25}$$

Then taking the difference of (14) and (22) leads to the state equation of $\partial\mathbf{P}(\cdot)$

$$\begin{aligned} \mathbf{e}_x(i+1) &= A(\mathbf{r})\mathbf{e}_x(i) + \Delta A(\mathbf{r},\mathbf{r}_m)\mathbf{y}_m(i) + \mathbf{e}_d(i) \\ \mathbf{e}(i) &= \mathbf{e}_x(i) + \mathbf{v}(i) \end{aligned}, \tag{26}$$

where $A(\mathbf{r})$ is the state matrix in (14), and the input matrix $\Delta A(\mathbf{r},\mathbf{r}_m)$ may be expanded as

$$\Delta A(\mathbf{r},\mathbf{r}_m) = A(\mathbf{r}) - A_c(\mathbf{r}_m) = \delta A_0 \nabla\alpha_i^2(\underline{\mathbf{r}})(\mathbf{r}-\mathbf{r}_m)(i) + \delta A_1(\mathbf{r}). \tag{27}$$

Expansion coefficients in (27) hold

$$\begin{aligned} \delta A_0 &= \begin{bmatrix} -1/2 & -1/6 \\ -1 & -1/2 \end{bmatrix},\ \delta A_1(\mathbf{r}) = o(\alpha_i^4) \\ \nabla\alpha_i^2(\underline{\mathbf{r}})(\mathbf{r}-\mathbf{r}_m) &\simeq -3\underline{\omega}_O^2 T^2 \underline{r}^{-2}\underline{\mathbf{r}}^T(\mathbf{r}-\mathbf{r}_m) \end{aligned}, \tag{28}$$

having defined $\underline{\mathbf{r}} = \gamma\mathbf{r} + (1-\gamma)\mathbf{r}_m$, with $0 \le \gamma \le 1$, so as to preserve equality in. (27). Note that the error dynamics $\partial\mathbf{P}(\cdot)$, being driven by the model output $\mathbf{y}_m$, modifies when the Embedded Model converts into a state observer, which is obtained by connecting the driving noise $\mathbf{w}$ to the model error $\mathbf{e}$ as in Fig. 1.

6 Noise Estimator and State Observer

When the driving noise $\mathbf{w}$ of the disturbance dynamics in (18) is estimated from the model error $\mathbf{e}$ in (26), the Embedded Model converts into a state observer, which allows estimating and predicting in real-time orbital and disturbance state variables.

6.1 State Prediction

State prediction is strictly related to the noise design ending into (18). As in Kalman filtering, model error $\mathbf{e}$ is the source for real-time estimating noise $\mathbf{w}$, or better, some causal combination of past values. Unlike classical predictors where driving noise is acting on each state variable, noise channels in (17) and (18) are preserved, which implies no driving noise directly perturbs the rate v_k as it is clear from (17). As explained in [5], such a constraint may require a dynamic noise estimator when

$$n_x = n_c + n_d > n_w \times n_y , \tag{29}$$

which is not the present case, since both position and rate measurements are available. A static noise estimator applies and holds

$$\bar{\mathbf{w}}(i) = L(i)\bar{\mathbf{e}}(i),\ \bar{\mathbf{e}}(i) = \mathbf{y}(i) - \hat{\mathbf{y}}_m(i) , \tag{30}$$

where

(i) bar and hat account for estimator inaccuracies to be treated below,

(ii) the gain matrix $L(i)$, sized $n_w \times n_y = 6 > n_x = 4$, must be time-varying to force closed-loop dynamics (model and noise estimator) to be LTI.

Since $L(i)$ is oversized with respect to state size in (23), some entries can be set to zero, while respecting stability. Denote the entries of $L(i)$ as follows

$$L(i) = \begin{bmatrix} l_{0r} & l_{0v} \\ l_{1r} & l_{1v} \\ l_{2r} & l_{2v} \end{bmatrix}(i) \tag{31}$$

and compute the characteristic polynomial $P(\gamma)$ of the state predictor

$$\begin{bmatrix}\hat{\mathbf{x}}_m\\ \hat{\mathbf{z}}_m\end{bmatrix}(i+1)=\begin{bmatrix}A_c(i)-G_cL(i) & H_c\\ -G_dL(i) & A_d\end{bmatrix}\begin{bmatrix}\hat{\mathbf{x}}_m\\ \hat{\mathbf{z}}_m\end{bmatrix}(i)+\begin{bmatrix}G_c\\ G_d\end{bmatrix}L(i)\mathbf{y}(i),\qquad \hat{\mathbf{y}}_m(i)=\hat{\mathbf{x}}_m(i)\,. \tag{32}$$

Straightforward computation, upon definition of $\gamma=1-\lambda$, λ denoting a generic eigenvalue, yields

$$\begin{aligned}&P(\gamma)=\gamma^4+c_3\gamma^3+c_2\gamma^2+c_1\gamma+c_0\\ &c_3=l_{ov}+\alpha_i^2\\ &c_2=l_{1v}+\left(\alpha_i^2+l_{0r}\right)\left(1-\alpha_i^2/4\right)+\left(\alpha_i^2/2+l_{ov}\right)\alpha_i^2/2\,,\\ &c_1=\left(1-\alpha_i^2/4\right)l_{1r}+l_{1v}\alpha_i^2/2+l_{2v}\\ &c_0=l_{2v}\alpha_i^2/2+\left(1-\alpha_i^2/4\right)l_{2r}\end{aligned} \tag{33}$$

where the polynomial coefficients, depending on the closed-loop eigenvalues λ_h, $h=1,\ldots,n_x$ are constant and possess a multiple of solutions. To find a unique solution, simplify (33) by setting $\alpha_i^2=0$, which leads to four equalities

$$\begin{aligned}&c_3\simeq l_{ov},\ c_2\simeq l_{1v}+l_{0r}\\ &c_1\simeq l_{2v}+l_{1r},\ c_0\simeq l_{2r}\end{aligned}\,. \tag{34}$$

Four alternative solutions of (34) exist, if useless coefficients are set to zero as in Table 3.

Table 3 Noise estimator alternative

Case	l_{1v}	l_{2v}	l_{0r}	l_{1r}	
0	0	0	X	X	Higher noise
1	0	X	X	0	Intermediate
2	X	0	0	X	Intermediate
3	X	X	0	0	Lower noise

X stands for not zero

Table 3 and (34) show that

(i) in the case 3, the rate measurement alone is sufficient for estimating all noise components;

(ii) the position measurement is necessary for guaranteeing closed-loop stability, as the last equation in (34) evinces.

Since position measurement is much noisier than rate as Table 1 shows, case 3 in Table 3 must be selected, as it agrees with the Kalman filtering guideline, proper of any measuring strategy, of reducing to a minimum any measurement noise passing through the noise-estimator feedback channels. A formal proof may be provided.

6.2 Predictor-Corrector scheme

Actually, prediction equation (32) can only be implemented with $L(i)=0$ because of the lower measurement rate $T_g^{-1} < T^{-1}$. This implies conversion to predictor-corrector scheme. Several schemes are possible. Denote with $t_j = jT_g$ the measurement times, such that $t_{i(j)} = t_j$ for $i(j) = n_g j$. At each time t_j the prediction correction is invoked

$$\begin{bmatrix} \overline{\mathbf{x}}_m \\ \overline{\mathbf{z}}_m \end{bmatrix}(j) = \begin{bmatrix} \hat{\mathbf{x}}_m \\ \hat{\mathbf{z}}_m \end{bmatrix}(i(j)) + \begin{bmatrix} K_c(j) \\ K_d(j) \end{bmatrix} \overline{\mathbf{e}}(i(j)), \tag{35}$$

where variable gains depend on the predictor gain $L(i(j))$ through

$$\begin{bmatrix} K_c(j) \\ K_d(j) \end{bmatrix} = \begin{bmatrix} A_c(i(j)) & H_c \\ 0 & A_d \end{bmatrix}^{-1} \begin{bmatrix} G_c \\ G_d \end{bmatrix} L(i(j)). \tag{36}$$

At each step i the predictor (30) is invoked with $L(i)=0$ and initial conditions

$$\hat{\mathbf{x}}_m(i(j)) = \overline{\mathbf{x}}_m(j),\ \hat{\mathbf{z}}_m(i(j)) = \overline{\mathbf{z}}_m(j). \tag{37}$$

Computing burden due to variable gains may be reduced either by decomposing the gain into steady and variable parts, or, more drastically, by reducing Eq. (22) to be LTI, which is obtained by treating the variable part of (13) as a known disturbance.

In the above scheme, asymptotic stability of the closed-loop state matrix in (32) is not sufficient to guarantee predictor-corrector stability, since, using notations in (22), the multi-step prediction matrix holds

$$F_h(j) = F(j)^h \left(F(j) - GL(j)C \right),\ h = 0,...,n_g - 1 . \tag{38}$$

The drawback may be circumvented by rewriting (33) in terms of the characteristic polynomial of $F_h(j),\ h = n_g - 1$. An alternative scheme, free of stability problems, is to implement (32) at each measurement time $t_j = jT_g$ and then interpolate during T_g.

6.3 Stability in presence of model uncertainty

According to (26), the neglected dynamics $\partial\mathbf{P}(\mathbf{y}_m,...)$ repeats the 'true' dynamics in Eq. (14) less a forcing error depending on $\mathbf{y}_m$, and due to approximate gravitational acceleration. Let us restrict to one-step predictor (32): though the predictor is forced through $L(i)$ to be asymptotically stable, the same cannot be said for the orbit prediction error $\hat{\mathbf{e}}_x = \mathbf{x} - \hat{\mathbf{x}}_m$, which replaces $\mathbf{e}_x$ in the error equation (26). Decomposition of $\hat{\mathbf{e}}_x$ into

$$\hat{\mathbf{e}}_x(i) = \mathbf{e}_x(i) + \mathbf{x}_m(i) - \hat{\mathbf{x}}_m(i) , \tag{39}$$

and combination of (26) with (32), converts the open-loop error dynamics (26) into

$$\begin{bmatrix} \hat{\mathbf{e}}_x \\ \hat{\mathbf{e}}_z \end{bmatrix}(i+1) = \begin{bmatrix} A_c(i) - G_c L(i) + \Delta A(\mathbf{r},\mathbf{r}_m) & H_c \\ -G_d L(i) & A_d \end{bmatrix} \begin{bmatrix} \hat{\mathbf{e}}_x \\ \hat{\mathbf{e}}_z \end{bmatrix}(i) + \begin{bmatrix} \Delta A(\mathbf{r},\mathbf{r}_m) \\ 0 \end{bmatrix} \hat{\mathbf{y}}_m(i) + \begin{bmatrix} I \\ 0 \end{bmatrix} \mathbf{e}_d(i) - \begin{bmatrix} G_c \\ G_d \end{bmatrix} L(i)\mathbf{v}(i) . \tag{40}$$

Stability of (40) is only affected by the structured uncertainty $\Delta A(\mathbf{r},\mathbf{r}_m)$, as it perturbs the stable predictor state matrix in (32): indeed, all forcing signals in (40) are bounded either because of predictor stability which is the case of $\Delta A(\mathbf{r},\mathbf{r}_m)\hat{\mathbf{y}}_m(i)$, or by construction, in which is the case of disturbance residual $\mathbf{e}_d(i)$, and of measurement noise $G_c L(i)\mathbf{v}(i)$. Stability of (40) may be guaranteed by different methods (see for instance [8] and [9]). In [4] and [10] stability is afforded by showing that the error dynamics (40) is the output of the open-loop error dynamics $\partial\mathbf{P}$ in (24), but filtered by the state predictor sensitivity $\mathbf{S}_m$, and by guaranteeing the harmonic inequality

$$\max_{|f|<f_{\max}} \left| \mathbf{S}_m(jf)\,\partial\mathbf{P}(jf) \right| \le \eta < 1,\ f_{\max} = 0.5/T_g , \tag{41}$$

where $|\cdot|$ is a suitable norm. Computation, omitted for brevity's sake, and simplification lead to

$$\max_{|f|<f_{\max}} \left| \mathbf{S}_m(jf)\,\partial\mathbf{P}(jf) \right| < \frac{f_O^2}{f_{\min}^2} < 1 , \tag{42}$$

where $f_{\min}$ is the predictor BW, which can be explicitly related to noise estimator gains in (31). Inequality (42) is consistent with the BW upper bound imposed by the measurement errors as shown in Section 7.

7 Simulated Results

Simulated results refer to GOCE mission during 42 hours (150 ks), that corresponds to about 30 orbits. Table 4 shows the a-posteriori error statistics (RMS) for the different LORF axes: the total RMS is shown together with the MBW and higher frequency components. Being a real-time estimate, low frequency residuals dominates due to the relevant components of the measurement errors which are integrated during the filter time constant, a fact that harmonic analysis, not treated here, would predict.

Table 4

LORF error RMS [μrad]

Axis	Total (target)	MBW	HF
x	0.48 (200)	0.08	0.001
y	4.0 (200)	0.8	0.03
z	1.6 (200)	0.04	0.03

The total RMS in Table 4 is largely lower than target in Table 2, showing filter efficiency. Figure 4 shows the time history of the along-track error: the MBW component is much lower than the total error as expected, being progressively attenuated by the filter narrow BW.

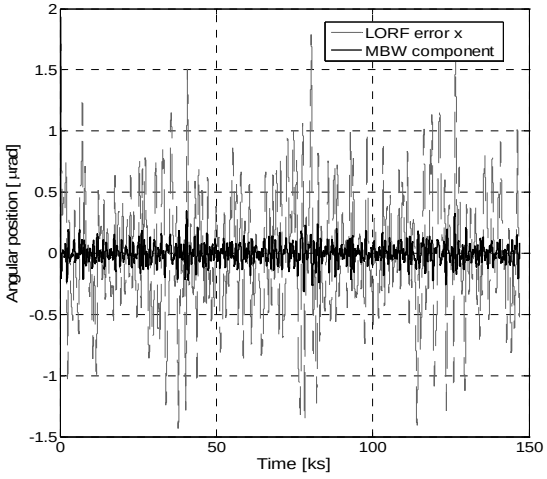

Fig. 4. LORF along-track error (x axis) and MBW component (narrow strip).

Considerations stemming from Fig. 4 are confirmed by the error PSD in Fig. 5, which shows a wide margin with respect to the target bound. Out-of-plane and radial (lateral) components overlap, whereas the along-track error appears much lower. The reason is due to different residual non-gravitational acceleration, which should be ideally zeroin case of a drag-free control acting on each axis. The latter is the case of the along-track axis, where low-frequency drag-free residuals are only due to accelerometer bias and drift. On the on the contrary, lateral non gravitational accelerations (see [5]) were not counteracted in the frequency region below the MBW for reasons of propellant saving. That implies radial and cross-track oscillations of the orbital motion, which have been deemed of no detriment to mission. Actually, having renounced to micro-propulsion [5], no lateral drag-free is performed on the GOCE satellite.

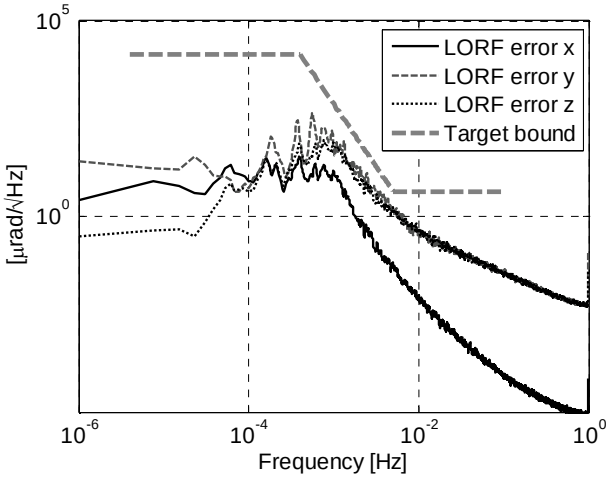

Fig. 5. LORF error PSD.

Figure 5 shows the observer BW to approach 1 mHz, close to the mean orbit frequency $\underline{f_O}$, because of the GPS measurement errors. Only accurate orbit and disturbance dynamics can cope with such a narrow BW and the stability inequality (42).

Figure 6 overlaps the pitch attitude with the corresponding LORF error; time unit is ks. Two mission phases are shown: in the former one, ending at about 80 ks, attitude is just measured by star trackers measurements, which are affected by large noise and bias; in the latter, data fusion between payload accelerometers and star trackers allows cancelling high frequency noise: bias of course remains.

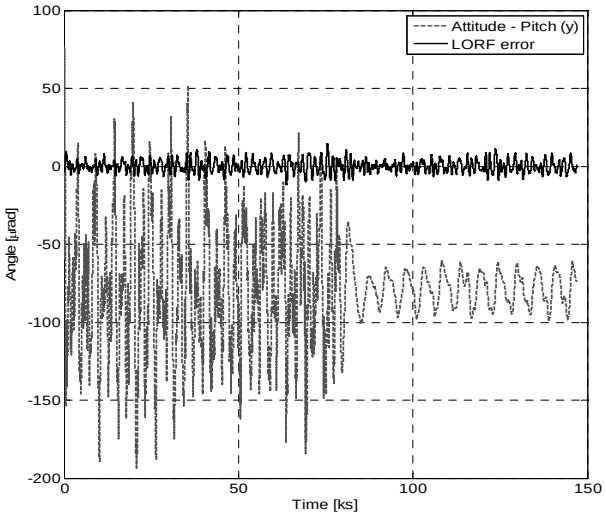

Fig. 6. Residual attitude and LORF error.

Acta Astronautica 66 (2010) 446 -- 454

8 Conclusion

A state predictor for the real-time estimation of the local orbital frame of drag-free LEO satellites was presented. It is designed as a predictor-corrector around an Embedded Model of the orbit dynamics relying on accurate controllable (orbit) and disturbance dynamics. Simulated results are compatible to GOCE target bounds, showing margin.

References

[1] Bertotti, B., and Farinella, P., *Physics of the Earth and the Solar System*. Dordrecht: Kluwer Academic Pu., 1990.

[2] Bisnath S. "Precise orbit determination of Low Earth Orbiters with a single GPS receiver-based, geometric strategy", Ph. D. dissertation, University of New Brunswick, February 2004.

[3] Canuto, E., P. Martella and G. Sechi G., "Attitude and drag control: an application to the GOCE satellite", *Space Science Reviews*, 2003, 108 (1-2), 357-366.

[4] Canuto, E., "Embedded Model Control: outline of the theory", *ISA Trans*. 46 (3), June 2007, pp. 363-377.

[4] Canuto, E., "Drag-free and attitude control for the GOCE satellite", *Automatica*, 44 (7), July 2008, pp. 1766-1780.

[5] Canuto, E.; and Massotti L., "All-propulsion design of the drag-free and attitude control of the European satellite GOCE", *Acta Astronautica*, 64, 2009, pp. 325-344, 2009.

[6] Kaplan, E.D. ed., *Understanding GPS: Principles and Applications*. Artech House Pu., Boston, 1996.

[7] Montenbruck, O. and Gill B. *Satellite Orbits. Models, Methods, Applications,* Springer-Verlag, Berlin, 2000.

[8] Chen, B-S. and Kung J-Y. "Robust stability of structured perturbation systems in state space model", in *Proc. 27th IEEE Conf. on Decision and Control,* Austin (Texas), pp. 121-122, 1988.

[9] Maciejowski, J. *Multivariable feedback design,* Addison.Wesley, 1989.

[10] Ospina J. "Embedded Model Control and the error loop", in *Proc. 8th International FLINS Conference*, Madrid (Spain), 22-24 September 2008, World Scientific Pu. (Singapore), pp. 975-980, 2008.